Authors' Accepted Manuscript - Thin-Walled Structures (2023)
https://doi.org/10.1016/j.tws.2023.110572

Engineered origami crease perforations for optimal mechanical performance and fatigue life

Yao Chen [a,*], Pan Shi [a], Yongtao Bai [b], Jiaqiang Li [a], Jian Feng [a], Pooya Sareh [c,d]

[a] *Key Laboratory of Concrete and Prestressed Concrete Structures of Ministry of Education, and National Prestress Engineering Research Center, Southeast University, Nanjing 211189, China*
[b] *School of Civil Engineering, Chongqing University, Chongqing 400044, China*
[c] *Creative Design Engineering Lab (Cdel), Department of Mechanical and Aerospace Engineering, School of Engineering, University of Liverpool, Liverpool, L69 3GH, United Kingdom*
[d] *Escuela Técnica Superior de Ingeniería y Diseño Industrial, Universidad Politécnica de Madrid (UPM), Rda. de Valencia, 3, 28012 Madrid, Spain*

Keywords:
Origami
Perforated crease
Mechanical characteristics
Fatigue prediction
Folding behavior

A B S T R A C T

Perforating crease lines has been widely adopted as a practical method for designing thick engineering origami structures. Perforations inevitably reduce crease stiffness and thus affects the mechanical characteristics and fatigue performance of origami structures. It is therefore important to understand the effect of perforations on the performance of origami creases. The purpose of this study is to propose a perforated crease with desirable folding response and fatigue performance for engineering origami structures. Drawing on the literature on engineering origami, ten perforated creases are proposed, including single- and double-sided slots, oblong holes, elongated holes, moon holes, and barbell holes. Next, finite element analysis is used to assess their folding and unfolding responses, and to predict their fatigue lives combined with FE-SAFE. It is demonstrated that the crease with three rows of oblong holes is the optimal design, which has excellent mechanical characteristics and fatigue performance. A parametric analysis is then carried out to investigate the effect of sheet thickness, hole size, and holes arrangement on the performance of the optimal perforated crease. It is revealed that increasing sheet thickness, hole distance, or row distance exerts a positive effect on reaction forces, while increasing hole length or hole width produces a negative effect. Additionally, the fatigue life is severely reduced as sheet thickness or hole length increases, while it enhances with increasing hole width or hole distance. On the other hand, variations in row distance have an insignificant effect on the fatigue life. The parametric analysis presented in this study can provide guidance for the application of optimal perforated creases to engineering origami structures.

1. Introduction

Origami, the ancient art of paper folding, has ongoingly inspired the design and development of a wide range of engineering structures with various desirable properties [1,2]. Examples include miniature manipulators [3,4], impact protection systems [5–7], deployable structures [8–12], energy absorption structures [13–15], and mechanical metamaterials [16,17]. Such origami-inspired engineering structures are commonly composed of thick materials such as polymers, metals, and composites. As a result, the problem of panel interference is introduced and analyzed [18], demonstrating the practical inability of conventional design methods based on the zero-thickness assumption [19–24] to accurately describe the folding behavior of origami structures. To deal with this problem, a diverse range of thick folding techniques has been proposed, among which perforating or cutting the crease lines during the manufacturing process is the most widely-used approach because of its ease of implementation and cost-efficiency.

Perforations create material discontinuities at the crease line and thus degrades the crease stiffness, which inevitably affects the mechanical properties of origami structures. It has been demonstrated that perforating a specific crease line could significantly reduce the bending force required to fold metal sheets, but produces localized high-stress regions around the perforations [25]. Notably, such stress-concentration areas may weaken the load-bearing capacity of folded metal sheets. For example, Ablat et al. [26] revealed that perforating the crease line affects the tension and shear load-bearing capacities of origami metal sheets and significantly reduces their average extensions. They also revealed that the hole shape is a key factor in determining the folding behavior of the origami sheets [27]. Similarly, Shi et al. [28] confirmed that hole shape could exert a substantial effect on

* Corresponding author.
E-mail address: chenyao@seu.edu.cn (Y. Chen).

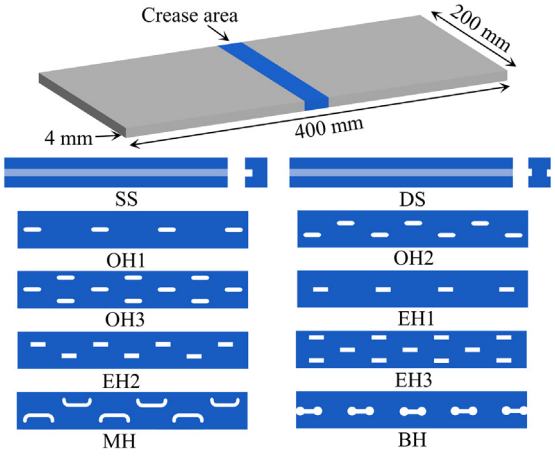

Fig. 1. Ten different crease-weakening schemes to be applied to the design of origami patterns.

the buckling behavior of folded hollow prismatic structures, according to the results of axial compression tests and finite element analyses. They afterward conducted a parametric experimental study to assess the interaction between hole shape and panel clash behavior [29]. In addition to hole shape, Ma et al. [30] showed that hole size (i.e., the ratio between the lengths of the long and short axes) affects the folding and unfolding performance of elliptical/rectangular holes-weakening creases, and reported that rectangular holes-weakening creases are difficult to be folded. Hwang [31] conducted a parametric analysis on the folding behavior of Kresling origami structures with perforated fold lines and found that hole arrangement plays a crucial role in determining the barrier force and spring constant of the structure. Some other studies have focused on the effect of hole shape and hole arrangement on the springback in sheet metal bending [32,33].

As mentioned above, most studies to date have focused on the reaction forces of perforated origami creases during folding. Other mechanical characteristics like energy absorption capacity and fatigue life have rarely been investigated, while they are of great significance for the practical application of origami structures. On the one hand, origami structures have been widely used in energy absorbing devices due to their excellent energy absorption performance [34,35]. Importantly, engineering origami structures typically experience frequent folding and unfolding processes during their lifetime, which may lead to fatigue failure [36–38]. Recent studies have revealed that crease design plays a vital role in maintaining the long fatigue life of origami structures [39,40]. More importantly, appropriately designed perforated crease lines could improve the fatigue resistance of origami structures [41]. Therefore, it is of particular importance to investigate the energy absorption capacity and fatigue performance of perforated origami creases to enable practical applications of engineering origami structures.

To investigate the abovementioned mechanical characteristics systematically, we propose ten perforated crease designs including single- and double-sided slots, oblong holes, elongated holes, moon holes, and barbell holes, which are inspired by [41,42]. Their associated cyclic folding and unfolding processes are then simulated using the finite element method to assess their mechanical characteristics including reaction forces, residual deformation, and special energy absorption. Next, we apply ABAQUS and FE-SAFE to predict the fatigue lives of the perforated creases. Theoretical fatigue lives are also calculated to verify the reliability of FE-SAFE predictions. Based on these analyses, an optimal perforated crease, i.e., the design with three rows of oblong holes, is identified. Finally, a parametric study is carried out to investigate the effect of sheet thickness, hole size, and holes arrangement on the mechanical characteristics of the identified perforated crease. It is expected that this perforated crease can be applied to designing origami patterns for practical engineering sapplications.

Table 1
Design parameters of slotted creases.

Parameters	SS	DS	OH1	OH2	OH3	EH1	EH2	EH3	MH	BH
w (mm)	6	6	2	1	1	2	1	1	0.5	1
l (mm)	200	200	5	5	3	6.6	5.4	3.4	3	3
c (mm)	/	/	10	9	11	8.4	9.6	10.6	8.5	5.8
d (mm)	/	/	/	3	3	/	3	3	/	/

2. Perforated crease design

Based on the existing research, we propose ten different crease-weakening schemes, including designs with single- and double-sided slots; one, two, and three row of oblong holes; one, two, and three row of elongated holes; moon holes; and barbell holes. They are hereinafter referred to as SS, DS, OH1, OH2, OH3, EH1, EH2, EH3, MH, and BH, respectively. Additionally, an unperforated origami crease (named 'no hole' or NH) is considered to explore the effect of perforations on the mechanical characteristics of the crease. As shown in Fig. 1, holes are slotted in the middle area of a rectangular metal sheet with dimensions of 400 mm × 200 mm × 4 mm. A slotted volume of 600 mm^3 is determined according to the principle of equal sheet volume. It should be noted that the dimensions adopted have been proven to facilitate the smooth folding of the metal sheet [30,43]. The detailed configurations are shown in Fig. 2 and the design parameters are listed in Table 1. In Fig. 2, h is the slot thickness, equal to 0.5 mm; l is the hole length; w is the hole width; c is the hole distance; d is the row distance; the two ends of the oblong hole are semicircles with a diameter equal to the hole width w; the ends of the moon hole are defined by a radius r_{MH} = 1.5 mm and a polar angle $\beta = 90°$; and the ends of the barbell hole are defined by a radius r_{BH} = 1.2 mm and a polar angle $\beta = 54°$.

3. Folding behavior

In this section, we investigate the folding and unfolding processes of various perforated origami creases using the finite element method (FEM). We aim to determine a perforated origami crease with highly desirable mechanical characteristics. In the following subsections, the cyclic loading simulations of perforated creases are first presented, followed by the simulation validation. Next, the folding responses of perforated creases are presented and discussed, including force–displacement curves, stress distributions, and mechanical indices.

3.1. Cyclic loading simulation

In this study, the cyclic folding and unfolding processes of the perforated origami creases are simulated using ABAQUS software. Fig. 3a shows a finite element model with OH3 as an example. All models adopt shell elements except SS and DS, which adopt the C3D8R elements. To ensure convergence and accuracy in simulation, the shell elements are mostly S4R, with a small number of S3R elements [44]. The left boundary is constrained for all degrees of freedom except the X-axis translation and Y-axis rotation, and the right boundary is set as hinged. A cyclic displacement-type loading along the X-axis with a step size of 1 s is applied to the reference point (RP-1) coupled to the left boundary, as designated by the blue arrow in Fig. 3a. The cyclic loading process is set to 0-320-5-320-5-320-5 mm (Fig. 3b). On the one hand, the simulation values of the sheet folding angle disagree with the theoretical values because of the large out-of-plane deformation occurring in the sheet during loading. As shown in Fig. 4, the folding angle of the metal sheet is approximately 3.29 rad (about 180°) when

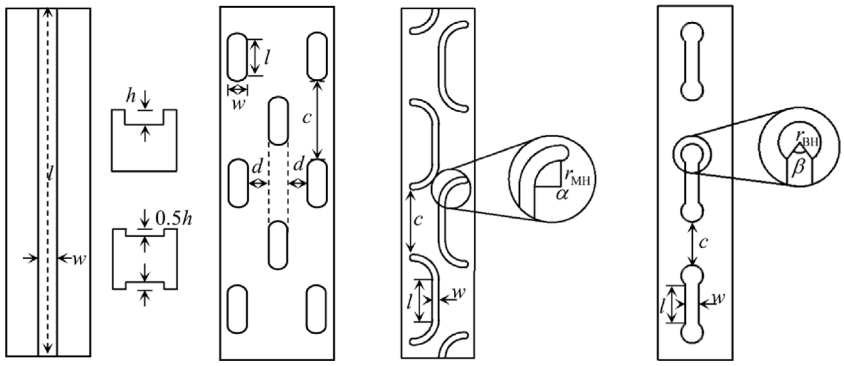

Fig. 2. Detailed configurations and parameters of different perforated creases.

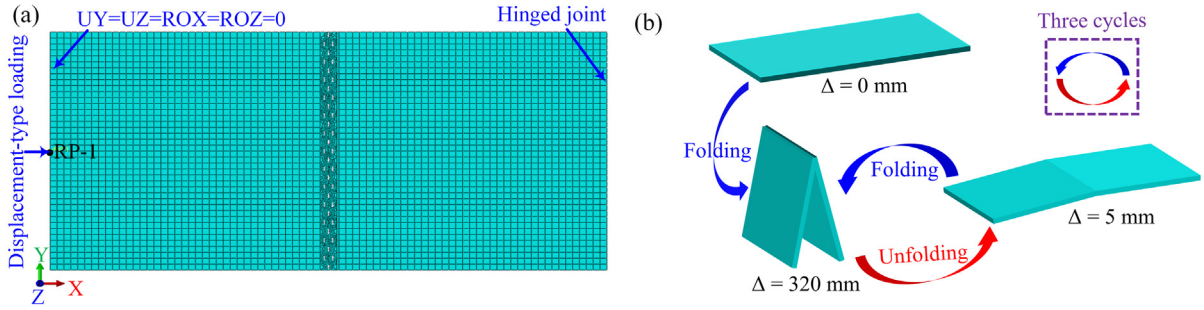

Fig. 3. Cyclic loading simulations of perforated origami creases. (a) Finite element model of OH3; (b) schematic diagram of the cyclic loading process. Δ denotes the loading displacement, and is defined as the X-axis distance that RP-1 deviates from its initial position after loading (For the interpretation of the references to colors in this figure, the reader is referred to the web version of this article.).

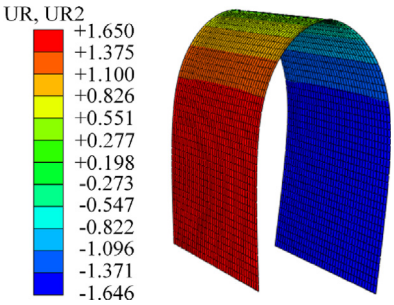

Fig. 4. Unit rotation angle of the unperforated origami sheet at the loading displacement of 320 mm.

the loading displacement reaches 320 mm. Hence, we take this value to assume that the metal sheet is fully folded. On the other hand, if the second and third minimum loading displacements are set to zero, extremely high stresses will be generated due to the residual deformation in the sheet. To avoid this, here we consider the value of 5 mm. Importantly, three loading cycles are sufficient to accurately analyze the folding behavior of the perforated origami creases [43]. Note that in order to faciliate the smooth folding of the metal sheet, a displacement of 1 mm along the positive Z-axis is imposed on the middle of the crease line before the cyclic loading.

The material of the metal sheet is Q235 steel, which has mechanical properties of density ρ = 7850 kg/m^3, Young's modulus E=206 GPa, Poisson's ratio ν=0.3, tensile strength σ_u = 400 MPa, yield strength σ_y = 235 MPa, and ultimate strain ε_u = 20% [43]. The trilinear hardening model is adopted to describe the constitutive relationship of the material.

3.2. Validation of simulations

To verify the reliability and accuracy of our simulations, we simulate the folding behavior of a double-sided slotted crease with the same geometric parameters reported in [43], i.e., a metal sheet with slot dimensions of $w \times h$ = 60 mm × 2 mm in Fig. 1. As shown in Fig. 5, our simulations are in reasonable agreement with the reported results. Both stress distributions exhibit a uniform strip shape, with the maximum stress distribution around the crease area. Our simulated force–displacement curves are fairly coincidental with those previously reported, and can accurately describe the experimental results. Therefore, it is verified that our simulations can describe the folding behavior of perforated origami creases with a good level of accuracy.

3.3. Force–displacement curves

Here, we first analyze the force–displacement curve of the unperforated metal sheet presented in Fig. 6a. It can be seen that the curve exhibits a stable hysteretic loop after the first loading cycle, which demonstrates that three loading cycles are sufficient to describe the cyclic folding and unfolding behavior of the metal sheet. The hysteretic loop becomes plumper with increasing the loading cycle, due to the residual deformation generated in the sheet, which manifests itself as an increase in the peak displacement. We can also observe that the reaction force at Δ = 320 mm increases as the loading cycle increases, indicating that the cyclic folding can lead to greater residual stresses in the fully-folded sheet [43].

Since the folding behavior of the metal sheet is stable, we only present the force–displacement curves for various perforated creases during the second folding and unfolding processes in Fig. 6b. It can be observed that the loop area of all perforated creases is reduced to varying degrees compared with NH, with MH in particular having the smallest loop area. The varying degrees of reduction suggest that the perforation geometry plays a crucial role in determining the folding response of the perforated sheet metal [27]. The main reason for this is the degradation of the crease stiffness caused by perforating the crease.

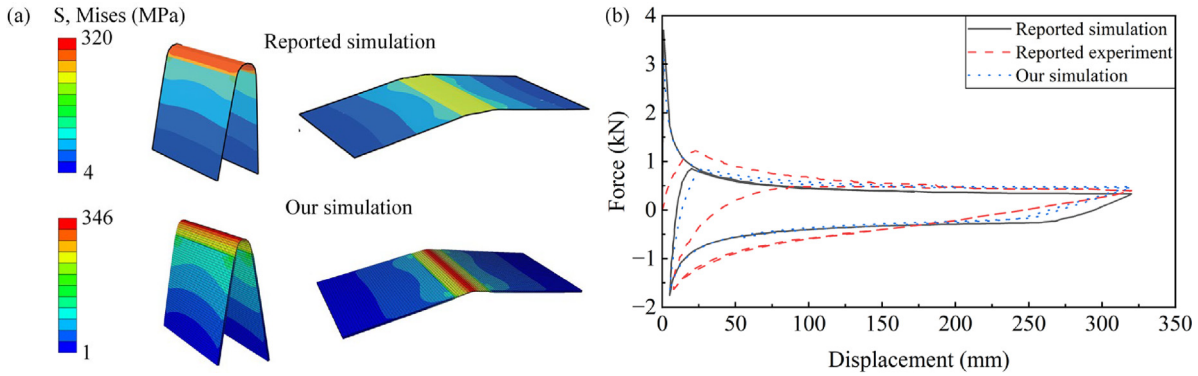

Fig. 5. (a) Von Mises stress distributions and (b) force–displacement curves of the double-sided slotted crease, compared with the results reported in [43].

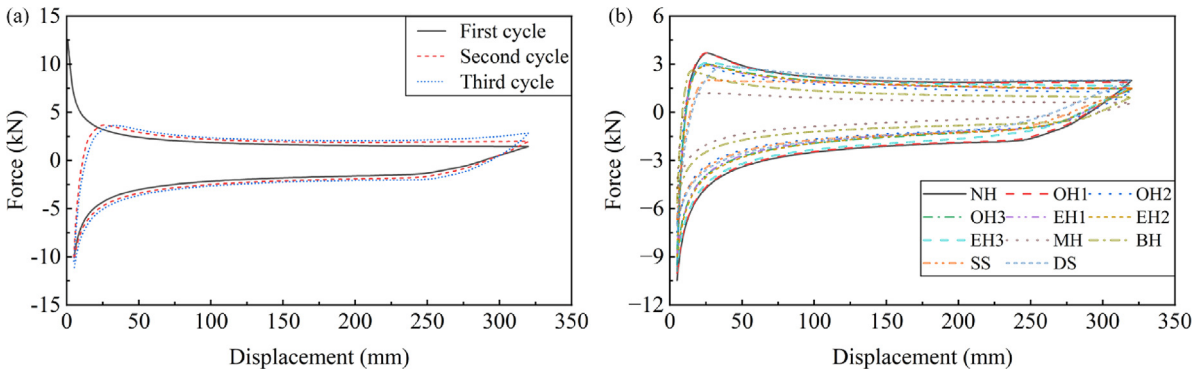

Fig. 6. Force–displacement curves of (a) NH and (b) various perforated origami creases.

3.4. The von Mises stress distributions

To further explore the effect of perforations on the folding responses of the metal sheets, we analyze their von Mises stress distributions during folding. For NH in Fig. 7a, a wide region of high stress is formed around the fold line, with a relatively small rotation arc around it. This indicates that the unperforated metal sheet is difficult to fully fold along the fold line. A similar observation is made for DS, although it has less stress in the crease area (Fig. 7c). In Fig. 7b, it can be observed that SS exhibits a shape of W and produces a pronounced stress concentration along the fold line. This is because the panels on either side of the slot contact and collision during folding, which in turn causes them to fold around their middle line. In contrast, OH1 not only enables the full folding of the metal sheet, but also greatly reduces the width of the high-stress region (Fig. 7d). As a result, in order to enable the full folding behavior of the metal sheet, the hole-weakening crease scheme is recommended over the cutting-weakening crease scheme.

We next analyze the von Mises stress distributions for various fully-unfolded metal sheets. Since SS and DS have poor folding behaviors, only the results for the holes-weakening creases are presented in Fig. 8. It can be seen that the stress distribution in all metal sheets is almost symmetrical with respect to the crease line [45,46]. Perforating the crease line could induce stress redistribution in the metal sheet, which has also been found in previous studies [25,30]. Except for EH3, all other perforated creases reduce the width of the high-stress zone to varying degrees. Among them, the high-stress zones of MH and BH are distributed entirely around the hole tips, reflecting the strong stress concentration phenomenon. This explains their least plump curves in Fig. 6b. Note that OH3 has the smoothest stress gradient, which manifests itself as a progressive change in color. The smooth stress gradient can ensure the smooth and full folding and unfolding processes of the origami metal sheet.

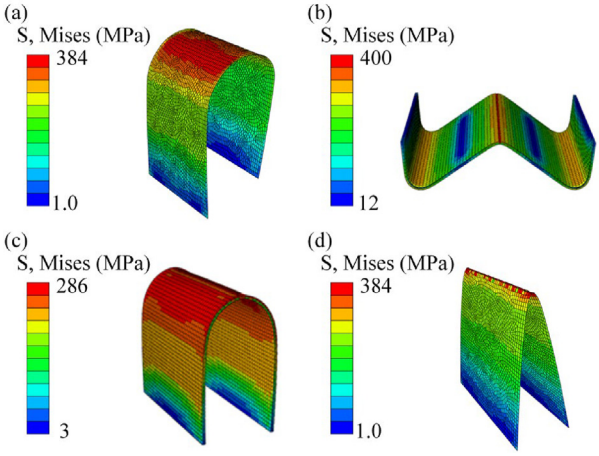

Fig. 7. The von Mises stress distributions of (a) NH, (b) SS, (c) DS, and (d) OH1 in their fully-folded states.

3.5. Mechanical indices

To quantitively characterize the mechanical properties of various perforated origami creases, we extract the maximum reaction force F_{ff} during the first folding, the maximum reaction force F_{aff} after the first folding, the maximum reaction force F_{uf} during unfolding, and the residual deformation δ from the force–displacement curves. Furthermore, we calculate the special energy absorption (SEA) to evaluate the energy absorption capacity of the structure. The SEA is defined as the energy absorbed per unit mass [47], as

$$\mathrm{SEA} = \frac{1}{m}\int_0^{\delta} F d\delta \tag{1}$$

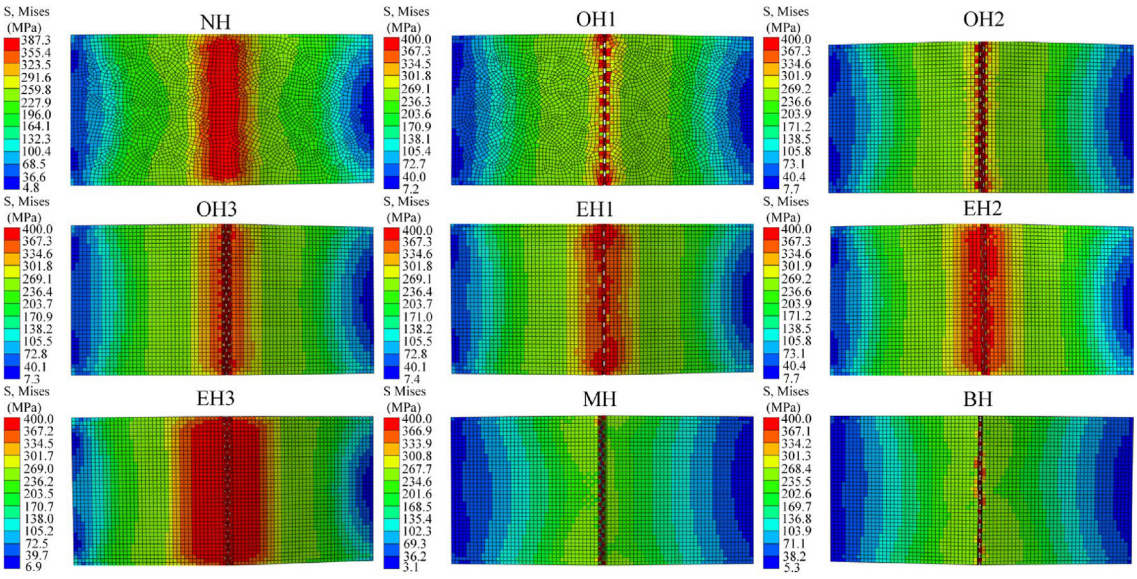

Fig. 8. The von Mises stress distributions of various fully-unfolded metal sheets.

Table 2
Mechanical properties of various perforated origami creases.

Crease type	NH	OH1	OH2	OH3	EH1	EH2	EH3	MH	BH
F_{ff} (kN)	12.56	12.38	11.25	11.60	12.02	11.81	11.97	7.27	11.15
F_{aff} (kN)	3.70	3.70	2.90	3.00	3.01	2.96	3.09	1.18	2.51
F_{uf} (-kN)	10.33	10.01	7.55	8.60	8.94	9.27	9.87	4.92	5.63
δ (mm)	11.14	10.00	10.54	11.15	10.54	12.04	13.27	9.60	8.87
SEA (10^{-3} J/g)	573.11	561.11	405.24	459.79	451.54	424.79	523.65	201.44	306.71

where δ is the axial displacement and m is the mass of the metal sheet.

Here we only list the mechanical indices of the holes-weakening creases in Table 2. It can be found that the mechanical indices of OH1 are fairly close to those of NH, mainly because one row of oblong holes has insignificant effect on the crease stiffness. In contrast, the crease stiffness of MH is severely degraded; as a result, its F_{ff}, F_{aff}, and F_{uf} are only about 58%, 32%, and 48% of NH, respectively. However, further degradation of the crease stiffness can reduce the residual deformation of the structure. As such, we obtain $\delta = 9.60$ mm and $\delta = 8.87$ mm for MH and BH, respectively, which are smaller than that of the other perforated creases. By comparing the SEA values, we can find that OH1, EH3, and OH3 rank in the top three in terms of energy absorption capacity. The SEAs of MH and BH are respectively only about 35% and 54% of NH, attributed to the severe degradation of the crease stiffness.

As discussed so far, it can be concluded that OH3 is a crease with excellent folding and unfolding responses. It can not only impart excellent mechanical properties to the metal sheet but also can enable its full folding and unfolding behavior. Although OH1 has the best mechanical indices, its stress concentration effect is stronger than that of OH3, which is also where OH2, MH, and BH fall short. The strong stress concentration generated at the crease lines is detrimental to the fatigue life of the structure, which will be discussed in the following section. EH1, EH2, and EH3 are not recommended because they do not have stress gradients as smooth as OH3, although some of their mechanical indices are better than OH3.

4. Fatigue life prediction

We have demonstrated that OH3 has an excellent folding and unfolding response. This section further examines whether it has a good fatigue performance using FE-SAFE and theoretical equations. Since SS and DS have been demonstrated not to enable the full folding behavior of the metal sheet, we do not predict their fatigue lives in this study. This section focuses on the fatigue cycle contours and fatigue lives of the proposed perforated origami creases.

4.1. Fatigue prediction approach

We carry out fatigue prediction based on ABAQUS and FE-SAFE. The local stress–strain approach [48] is adopted because the crease, as the most unfavorable position, determines the fatigue life of the metal sheet. This approach can also consider the loading sequence, thus providing more precise computations. First, the cyclic loading simulations of the perforated origami creases are carried out using ABAQUS. The simulation details can be seen in Section 3.1, but here the loading process is set to 0-10-5-10-5-10-5 mm. The different loading setting is because a great loading displacement of 320 mm could lead to a one-off failure of the structure. Then, the finite element results (ODB suffix files) are imported into FE-SAFE for fatigue analysis using the *E-N* approach, combined with Morrow's mean stress correction [49], the rain-flow counting method [50], and the cumulative damage theory [51]. Note that in FE-SAFE, the parameters for material properties and loading processes need to be reset. Finally, the fatigue prediction results (ODB suffix files) are imported into ABAQUS to obtain the fatigue cycle contours of the perforated origami creases.

To verify the reliability and accuracy of the FE-SAFE predictions, we calculate the theoretical fatigue lives of the perforated origami creases by the Manson–Coffin relation [49]:

$$\varepsilon_a = \varepsilon_{ea} + \varepsilon_{pa} = \frac{\sigma'_f}{E}(2N)^b + \varepsilon'_f(2N)^c \tag{2}$$

where ε_a, ε_{ea} and ε_{pa} are total, elastic, and plastic strain range respectively, σ'_f denotes fatigue strength, ε'_f denotes fatigue ductility, b and c are exponents of fatigue strength and ductility respectively, and N is number of cycles to failure. These coefficients are determined according to the Seeger algorithm [52]. As such, we obtain Eq. (3) to calculate the theoretical fatigue lives of the perforated origami creases.

$$\varepsilon_a = 0.003(2N)^{-0.08} + 0.1559(2N)^{-0.462} \tag{3}$$

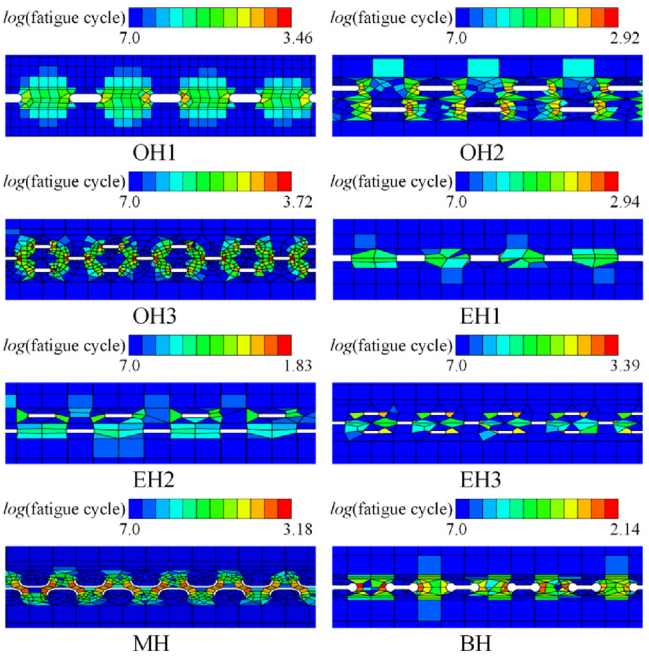

Fig. 9. Fatigue life contours of various perforated origami creases.

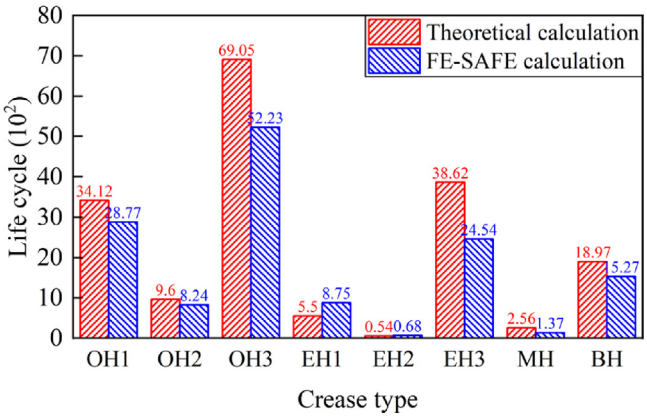

Fig. 10. Fatigue lives of various perforated origami creases.

Table 3
Base values and a full list of values for each parameter under study.

Parameters	Baseline value	A full list of values
t (mm)	4.0	4.0, 5.0, 6.0, 7.0, 8.0
l (mm)	3.0	2.0, 3.0, 4.0, 5.0, 6.0
w (mm)	1.0	0.5, 1.0, 1.5, 2.0, 2.5
c (mm)	11.0	8.0, 9.0, 10.0, 11.0, 12.0
d (mm)	2.0	1.0, 1.5, 2.0, 2.5, 3.0

4.2. Fatigue life contour

Since the number of fatigue cycle of the panel area is much greater than that of the crease area, we only display the fatigue life contours of the crease area in Fig. 9. It can be observed that the regions with low fatigue cycles are mainly distributed around the tips of the holes, indicating that fatigue failure commonly occurs in the most unfavorable position, i.e., the stress concentration zone. For MH, the regions with low fatigue cycles are connected at the intersection of the holes, forming wavy ribbons. On the other hand, for the other perforated creases, the regions with low fatigue cycles are separated from each other and displayed as dots. The dotted regions might be broken due to continuous cyclic folding, but this breakage does not cause the failure of the crease. Thus, the metal sheet can still fold and unfold against the crease line. We can also observe that the lowest fatigue cycle for OH3 is about $10^{3.7}$, which is much greater than that of the other perforated origami creases. This means that the crease with three rows of oblong holes can experience frequent folding and unfolding processes over long periods of time, that is, OH3 has the best fatigue performance.

4.3. Fatigue life

Fig. 10 shows the fatigue life of various perforated origami creases using theoretical equations and FE-SAFE. The fatigue lives predicted by FE-SAFE are approximately close to the theoretical calculations, indicating that FE-SAFE can provide reliable and accurate fatigue predictions. The calculation difference is because the theoretical formulae ignore the roughness between the contact surfaces. Both theoretical calculations and simulations show that OH3 has the longest fatigue life. It can be explained that the three rows of oblong holes can induce progressive stress distribution in the metal sheet and avoid excessive concentrated stresses at the crease line, as described in Section 3.4. For the other perforated creases, either the concentrated stress around the crease is relatively great, or the stress distribution is unsmooth. Consequently, their fatigue lives, particularly EH1, EH2, and MH, are much lower than OH3.

Overall, considering this analysis along with the analysis presented in Section 3, it can be concluded that OH3 is the optimal crease design.

5. Parametric analysis

We have so far identified a perforated origami crease with excellent folding and unfolding responses and the longest fatigue life, i.e., the three rows of oblong holes. To further understand the effect of sheet thickness, hole size, and holes arrangement on its mechanical behavior and fatigue performance, a parametric analysis is carried out, taking into account sheet thickness t, hole length l, hole width w, hole distance c, and row distance d. Accordingly, a total of 21 different three rows of oblong holes are constructed. Their design parameters are listed in Table 3, where the design parameters listed in Table 1 for OH3 are taken as the baseline values.

Fig. 11 shows F_{ff}, F_{aff}, F_{uf}, SEA, and fatigue life versus different design parameters. OH3base corresponds to OH3 taking the baseline value whereas OH3t50 corresponds to OH3 with a sheet thickness of 5 mm, the denotation of which is similar to that of other abbreviations. In Fig. 11a–e, the dimensionless values are the ratios of the respective values of each perforated crease and OH3base.

5.1. Parametric analysis on mechanical characteristics

In Fig. 11a, F_{ff}, F_{aff}, F_{uf}, and SEA increase almost linearly with the sheet thickness, with the slope of the curve for F_{ff} being the greatest. This is mainly because the crease stiffness increases exponentially with the sheet thickness. When the sheet thickness increases from 4 mm (OH3base) to 8 mm (OH3t80), the corresponding F_{ff}, F_{aff}, F_{uf}, and SEA increase by 5.99, 4.68, 4.64, and 2.54 times, respectively. This suggests that thicker sheets are conducive to improving the mechanical characteristics of the perforated origami crease. Nevertheless, if the metal sheet is too thick, the sheet cannot be fully folded against the crease line due to the panel clash behavior [29]. More importantly, thicker sheets are detrimental to their fatigue performance (Fig. 11f), which will be discussed later. Hence, determining the sheet thickness should take into account mechanical properties, folding behavior, and fatigue performance.

In Fig. 1b, all the curves show an approximately linear downward trend as the hole length increases. The reason is that increasing the hole length leads to a larger hole volume and thus degrades the crease stiffness. In previous studies, it has been demonstrated that the maximum

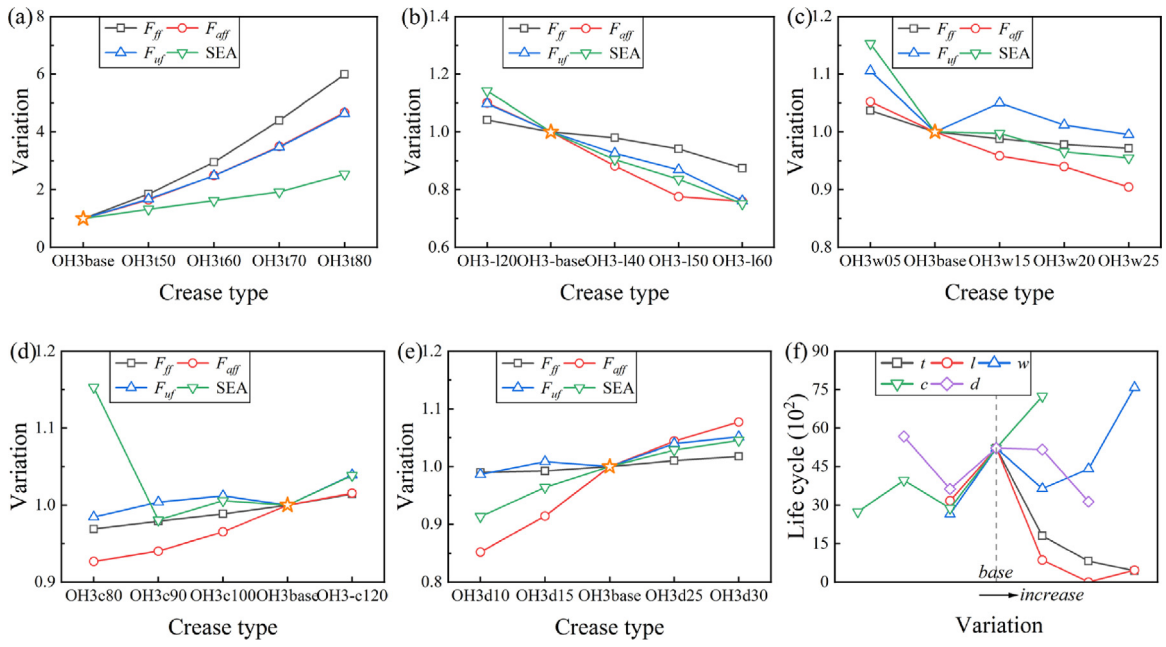

Fig. 11. Mechanical properties versus different design parameters: (a) sheet thickness t; (b) hole length l; (c) hole width w; (d) hole distance c; (e) row distance d; and (f) fatigue life.

bending force of perforated metal sheets are negatively correlated with the hole volume [27,30,53]. Likewise, wider holes result in the degradation of the crease stiffness. Thus, the mechanical properties of OH3 gradually decline with the hole width (Fig. 11c). Note that changes in mechanical properties are less sensitive to the hole width than the hole length, which is consistent with the reported simulations [30]. Similarly, the greater the value of hole distance c, the smaller the hole volume. As a result, the crease stiffness is enhanced, which improves the mechanical properties of OH3 (Fig. 11d). It is worth noting that the SEA of OH3c20 is the largest, whereas its F_{ff}, F_{aff}, and F_{uf} are slightly lower than that of OH3base. This means that the energy absorption capacity of a perforated origami crease can be improved by reducing the hole distance. In Fig. 11e, the mechanical properties of OH3 are improved to varying degrees with the row distance. This is because increasing the row distance widens the crease region and thus enhances the crease stiffness.

In general, increasing the sheet thickness, hole distance, or row distance exerts a positive influence on the mechanical properties of the three rows of oblong holes, whereas increasing the hole length or hole width produces a negative effect.

5.2. Parametric analysis on the fatigue life

Fig. 11f shows the number of fatigue cycles versus various design parameters. The fatigue life of OH3 is sensitive to variations in sheet thickness and hole length. When the sheet thickness increases from 4 mm to 8 mm, the fatigue cycle is reduced by 95%; when the hole length is 5 mm, the number of fatigue cycles equals 6, which is much smaller than OH3base (5223 cycles). These results indicate that we must be cautious with determining the sheet thickness and hole length. For the hole width, the curve of fatigue life shows an overall upward trend. When the hole distance is less than 3.5 mm, the fatigue life is lower than that of the OH3base and remains almost unchanged. Nevertheless, with a further increase in the hole distance, the fatigue life begins to increase. For the row distance, the curve is relatively smooth, indicating that variation in the row distance produces an insignificant effect on the fatigue life of OH3.

Fig. 12 presents the fatigue life contours of OH3 with various design parameters. The fatigue life contours of OH3base can be seen in Fig. 9. For all cases, the lowest fatigue life regions are distributed around the crack tips, i.e., the stress concentration zones. As the sheet thickness increases, the low fatigue cycle area spreads throughout the entire crease line and even extends into the panel (Fig. 12a). As described previously, a thicker sheet is difficult to fold against the crease line. As a result, a wide high-stress zone can be easily formed around the crease line, which is detrimental to the fatigue life of the metal sheet. These results illustrate the drop-off curve of the sheet thickness in Fig. 11f. In Fig. 12b, the stress concentration around the hole tips is strengthened as the hole length increases. Especially when the hole length is 5 mm, the stress concentration zones between adjacent holes are interconnected (shown in red), resulting in the fatigue failure of the entire crease line. Conversely, wider holes can weaken the concentrated stress around the hole tips (Fig. 12c). Therefore, the fatigue performance of the metal sheet is improved with the hole width. Likewise, increasing the hole distance can reduce concentrated stresses, resulting in the improvement of fatigue behavior (Fig. 12d). In Fig. 12e, the lowest fatigue cycle remains almost unchanged with the row distance, which is consistent with the curve change in Fig. 11f.

According to the above parametric analysis, it is demonstrated that there should be a set of design parameters that can impart the best mechanical properties and fatigue performance to the three rows of oblong holes.

6. Conclusions

In this study, ten weakening crease schemes were proposed for non-zero thickness origami structures, including single- and double-sided slots; 1, 2, and 3 rows of oblong holes; 1, 2, and 3 rows of elongated holes; moon holes; and barbell holes. Their full folding and unfolding responses under cyclic loading were investigated using FEM. Besides, FE-SAFE and theoretical equations were employed to predict their fatigue lives. The mechanical properties, energy absorption characteristics, and fatigue lives of the perforated creases were obtained to the most desirable crease design. The results show that the crease with three rows of oblong holes is the optimal crease design, inducing

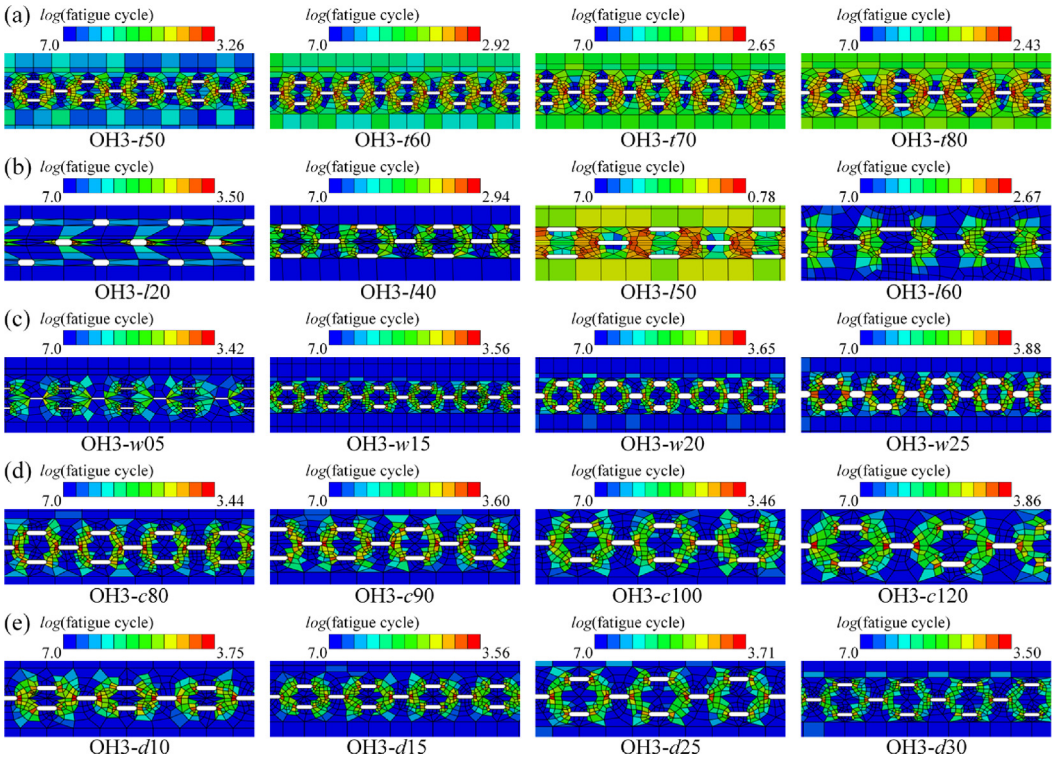

Fig. 12. Fatigue life contours for three rows of oblong holes with different design parameters: (a) sheet thickness t; (b) hole length l; (c) hole width w; (d) hole distance c; and (e) row distance d (For the interpretation of the references to colors in this figure, the reader is referred to the web version of this article.).

a smooth stress distribution in the metal sheet without excessive stress concentrations at the crease line. Hence, it not only has excellent mechanical properties but also possesses the best fatigue performance. It is demonstrated that this perforated crease is an appropriate design choice for engineering origami structures.

We further conducted a parametric study on the mechanical properties and fatigue lives of the optimal perforated crease (OH3). Systematic variations in sheet thickness, hole length, hole with, hole distance, and row distance were considered. The results show that increasing sheet thickness, hole distance, or row distance exerts a positive influence on the mechanical properties of OH3, whereas increasing hole length or hole width has a negative effect. Moreover, the fatigue life of OH3 is sensitive to variations in sheet thickness and hole length; when the sheet thickness or hole length is doubled, the number of fatigue cycles is massively reduced, which demonstrates the importance of sheet thickness and hole length as crucial design parameters for origami structures. In particular, due to the reduction of stress concentration, increasing hole width and hole distance can improve the fatigue life of OH3, whereas variations in row distance exerts an insignificant effect on it. In a word, the parametric analysis can provide guidance for the application of the proposed optimal perforated crease to the design of engineering origami structures.

CRediT authorship contribution statement

Yao Chen: Writing – review & editing, Writing – original draft, Validation, Supervision, Methodology, Funding acquisition, Formal analysis, Conceptualization. **Pan Shi:** Writing – original draft, Visualization, Validation, Software, Methodology, Formal analysis, Data curation. **Yongtao Bai:** Writing – review & editing, Supervision, Investigation, Conceptualization. **Jiaqiang Li:** Writing – original draft, Visualization, Software, Methodology, Formal analysis, Data curation, Conceptualization. **Jian Feng:** Writing – review & editing, Validation, Supervision, Funding acquisition, Conceptualization. **Pooya Sareh:** Writing – review & editing, Visualization, Validation, Supervision, Investigation, Funding acquisition, Conceptualization.

Declaration of competing interest

The authors declare that they have no known competing financial interests or personal relationships that could have appeared to influence the work reported in this paper.

Data availability

Data will be made available on request.

Acknowledgments

This work has been supported by the National Natural Science Foundation of China (Grants No. 51978150 and 52050410334), Southeast University "Zhongying Young Scholars" Project, and the Fundamental Research Funds for the Central Universities. The first author and the third author would like to acknowledge financial support from the Alexander von Humboldt-Foundation, Germany for their academic research respectively at Max–Planck-Institut für Eisenforschung GmbH and Leibniz University of Hannover, Germany. The authors are grateful to the editors and anonymous reviewers for their professional comments and valuable suggestions in improving the quality of the paper.

References

[1] Z. Zhai, L. Wu, H. Jiang, Mechanical metamaterials based on origami and kirigami, Appl. Phys. Rev. 8 (2021) 041319, http://dx.doi.org/10.1063/5.0051088.

[2] S. Li, H. Fang, S. Sadeghi, P. Bhovad, K.W. Wang, Architected origami materials: How folding creates sophisticated mechanical properties, Adv. Mater. 31 (2019) 1805282, http://dx.doi.org/10.1002/adma.201805282.

[3] H. Suzuki, R.J. Wood, Origami-inspired miniature manipulator for teleoperated microsurgery, Nat. Mach. Intell. 2 (2020) 437–446, http://dx.doi.org/10.1038/s42256-020-0203-4.

[4] T. Weinstein, H. Gilon, O. Filc, C. Sammartino, B.E. Pinchasik, Automated manipulation of miniature objects underwater using air capillary bridges: pick-and-place, surface cleaning, and underwater origami, ACS Appl. Mater. Interfaces 14 (2022) 9855–9863, http://dx.doi.org/10.1021/acsami.1c23845.

[5] J.A. Harris, G.J. McShane, Impact response of metallic stacked origami cellular materials, Int. J. Impact Eng. 147 (2021) http://dx.doi.org/10.1016/j.ijimpeng.2020.103730.

[6] P. Sareh, P. Chermprayong, M. Emmanuelli, H. Nadeem, M. Kovac, Rotorigami: A rotary origami protective system for robotic rotorcraft, Sci. Robot. 3 (2018) eaah5228, http://dx.doi.org/10.1126/scirobotics.aah5228.

[7] P. Sareh, P. Chermprayong, M. Emmanuelli, H. Nadeem, M. Kovac, The spinning cyclic 'Miura-oRing' for mechanical collision-resilience, Origami 7 (3) (2018) 981–994.

[8] T. Chen, O.R. Bilal, R. Lang, C. Daraio, K. Shea, Autonomous deployment of a solar panel using elastic origami and distributed shape-memory-polymer actuators, Phys. Rev. A 11 (2019) 064069, http://dx.doi.org/10.1103/PhysRevApplied.11.064069.

[9] J. Morgan, S.P. Magleby, L.L. Howell, An approach to designing origami-adapted aerospace mechanisms, J. Mech. Des. 138 (2016) 052301, http://dx.doi.org/10.1115/1.4032973.

[10] R.J. Lang, Twists, tilings, and tessellations: mathematical methods for geometric origami, CRC Press, Boca Raton, FL, 2018.

[11] T. Nojima, Modelling of Folding Patterns in Flat Membranes and Cylinders by Origami, JSME International Journal Series C 45 (1) (2002) 364–370.

[12] P. Sareh, S.D. Guest, Design of non-isomorphic symmetric descendants of the Miura-ori, Smart Materials and Structures 24 (8) (2015) 085002, http://dx.doi.org/10.1088/0964-1726/24/8/085002.

[13] X.M. Xiang, G. Lu, Z. You, Energy absorption of origami inspired structures and materials, Thin-Walled Struct. 157 (2020) 107130, http://dx.doi.org/10.1016/j.tws.2020.107130.

[14] J. Li, Y. Chen, X. Feng, J. Feng, P. Sareh, Computational modeling and energy absorption behavior of thin-walled tubes with the Kresling origami pattern, J. Int. Assoc. Shell Spat. Struct. 62 (2021) 71–81, http://dx.doi.org/10.20898/j.iass.2021.008.

[15] K. Yang, S. Xu, J. Shen, S. Zhou, Y.M. Xie, Energy absorption of thin-walled tubes with pre-folded origami patterns: Numerical simulation and experimental verification, Thin-Walled Struct. 103 (2016) 33–44, http://dx.doi.org/10.1016/j.tws.2016.02.007.

[16] X. Xiang, W. Qiang, B. Hou, P. Tran, G. Lu, Quasi-static and dynamic mechanical properties of Miura-ori metamaterials, Thin-Walled Struct. 157 (2020) 106993, http://dx.doi.org/10.1016/j.tws.2020.106993.

[17] S. Zhao, Y. Zhang, Y. Zhang, J. Yang, S. Kitipornchai, A functionally graded auxetic metamaterial beam with tunable nonlinear free vibration characteristics via graphene origami, Thin-Walled Struct. 181 (2022) 109997, http://dx.doi.org/10.1016/j.tws.2022.109997.

[18] R.J. Lang, K.A. Tolman, E.B. Crampton, S.P. Magleby, L.L. Howell, A review of thickness-accommodation techniques in origami-inspired engineering, Appl. Mech. Rev. 70 (2018) 010805, http://dx.doi.org/10.1115/1.4039314.

[19] Z.Y. Wei, Z.V. Guo, L. Dudte, H.Y. Liang, L. Mahadevan, Geometric mechanics of periodic pleated origami, Phys. Rev. Lett. 110 (2013) 215501, http://dx.doi.org/10.1103/PhysRevLett.110.215501.

[20] Y. Chen, L. Fan, Y. Bai, J. Feng, P. Sareh, Assigning mountain-valley fold lines of flat-foldable origami patterns based on graph theory and mixed-integer linear programming, Comput. Struct. 239 (2020) 106328, http://dx.doi.org/10.1016/j.compstruc.2020.106328.

[21] Y. Chen, P. Sareh, J. Yan, A.S. Fallah, J. Feng, An integrated geometric-graph-theoretic approach to representing origami structures and their corresponding truss frameworks, J. Mech. Des. 141 (2019) 091402, http://dx.doi.org/10.1115/1.4042791.

[22] Y. Chen, C. Lu, J. Yan, J. Feng, P. Sareh, Intelligent computational design of scalene-faceted flat-foldable tessellations, J. Comput. Des. Eng. 9 (2022) 1765–1774, http://dx.doi.org/10.1093/jcde/qwac082.

[23] S. Li, K.W. Wang, Fluidic origami: a plant-inspired adaptive structure with shape morphing and stiffness tuning, Smart Mater. Struct. 24 (2015) http://dx.doi.org/10.1088/0964-1726/24/10/105031.

[24] P. Sareh, The least symmetric crystallographic derivative of the developable double corrugation surface: Computational design using underlying conic and cubic curves, Materials & Design 183 (2019) 108128, http://dx.doi.org/10.1016/j.matdes.2019.108128.

[25] M.A. Ablat, A. Qattawi, Finite element analysis of origami-based sheet metal folding process, J. Eng. Mater. Technol. 140 (2018) http://dx.doi.org/10.1115/1.4039505.

[26] M.A. Ablat, A.A. Alafaghani, J.Q. Sun, A. Qattawi, Experimental evaluation of tension and shear responses of material discontinuities in origami-based sheet metal bending, J. Eng. Mater. Technol. 144 (2022) http://dx.doi.org/10.1115/1.4053145.

[27] M. Ali Ablat, A. Qattawi, Investigating the design and process parameters of folded perforated sheet metal, Int. J. Adv. Manuf. Technol. 102 (2019) 615–633, http://dx.doi.org/10.1007/s00170-018-3149-5.

[28] Q. Shi, X. Shi, J.M. Gattas, S. Kitipornchai, Folded assembly methods for thin-walled steel structures, J. Construct. Steel Res. 138 (2017) 235–245, http://dx.doi.org/10.1016/j.jcsr.2017.07.010.

[29] Q. Shi, M.T. Heitzmann, J.M. Gattas, Nonlinear rotational stiffness and clash prevention in perforated steel fold lines, Eng. Struct. 209 (2020) 110218, http://dx.doi.org/10.1016/j.engstruct.2020.110218.

[30] W. Ma, X. Liu, X. Qiu, Y. Zhou, Y. Liu, W. Fu, X. Guo, Z. Qian, K. Du, J. Cai, Comparative folding/unfolding performance of notch-type compliant joints, Case Stud. Constr. Mater. (2022) e01760, http://dx.doi.org/10.1016/j.cscm.2022.e01760.

[31] H.Y. Hwang, Effects of perforated crease line design on mechanical behaviors of origami structures, Int. J. Solids Struct. 230–231 (2021) 111158, http://dx.doi.org/10.1016/j.ijsolstr.2021.111158.

[32] C.P. Nikhare, N. Kotkunde, S.K. Singh, Effect of material discontinuity on springback in sheet metal bending, Adv. Mater. Process. Technol. (2021) 1–20, http://dx.doi.org/10.1080/2374068X.2021.1953925.

[33] V. Nasrollahi, B. Arezoo, Prediction of springback in sheet metal components with holes on the bending area, using experiments, finite element and neural networks, Mater. Des. 1980-2015 36 (2012) 331–336, http://dx.doi.org/10.1016/j.matdes.2011.11.039.

[34] X.M. Xiang, G. Lu, Z. You, Energy absorption of origami inspired structures and materials, Thin-Walled Struct. 157 (2020) 107130, http://dx.doi.org/10.1016/j.tws.2020.107130.

[35] J. Ma, S. Chai, Y. Chen, Geometric design, deformation mode, and energy absorption of patterned thin-walled structures, Mech. Mater. 168 (2022) 104269, http://dx.doi.org/10.1016/j.mechmat.2022.104269.

[36] D. Jeong, K. Lee, Design and analysis of an origami-based three-finger manipulator, Robotica 36 (2018) 261–274, http://dx.doi.org/10.1017/S0263574717000340.

[37] Y. Bai, D.C. Nardi, X. Zhou, R.A. Picón, J. Flórez-López, A new comprehensive model of damage for flexural subassemblies prone to fatigue, Comput. Struct. 256 (2021) 106639, http://dx.doi.org/10.1016/j.compstruc.2021.106639.

[38] M.A. Wagner, J.-L. Huang, P. Okle, J. Paik, R. Spolenak, Hinges for origami-inspired structures by multimaterial additive manufacturing, Mater. Des. 191 (2020) 108643, http://dx.doi.org/10.1016/j.matdes.2020.108643.

[39] M. Moshtaghzadeh, Prediction of fatigue life of a flexible foldable origami antenna with Kresling pattern, Eng. Struct. 251 (2022) 113399, http://dx.doi.org/10.1016/j.engstruct.2021.113399.

[40] M. Moshtaghzadeh, A. Bakhtiari, E. Izadpanahi, P. Mardanpour, Artificial Neural Network for the prediction of fatigue life of a flexible foldable origami antenna with Kresling pattern, Thin-Walled Struct. 174 (2022) 109160, http://dx.doi.org/10.1016/j.tws.2022.109160.

[41] Max W. Durney, A.D. Pendley, Precision-folded, high strength, fatigue-resistant structures and sheet therefor, US, 8377566 B2, 2013.

[42] B. Gitlin, A. Kveton, H. Lalvani, Method of bending sheet metal to form three-dimensional structures, US, 6640605 B2, 2002.

[43] Q. Zhang, Y. Li, A.B. Kueh, Z. Qian, J. Cai, Folding responses of origami-inspired structures connected by groove compliant joints, J. Mech. Robot. 14 (2021) http://dx.doi.org/10.1115/1.4052803.

[44] J. Ma, Z. You, Energy absorption of thin-walled beams with a pre-folded origami pattern, Thin-Walled Struct. 73 (2013) 198–206, http://dx.doi.org/10.1016/j.tws.2013.08.001.

[45] P. Zhang, W. Fan, Y. Chen, J. Feng, P. Sareh, Structural symmetry recognition in planar structures using Convolutional Neural Networks, Eng. Struct. 260 (2022) 114227, http://dx.doi.org/10.1016/j.engstruct.2022.114227.

[46] A. Zingoni, Symmetry recognition in group-theoretic computational schemes for complex structural systems, Comput. Struct. 94–95 (2012) 34–44, http://dx.doi.org/10.1016/j.compstruc.2011.12.004.

[47] G. Lu, T. Yu, Energy Absorption of Structures and Materials, Elsevier, 2003.

[48] D.F. Socie, Fatigue-life prediction using local stress–strain concepts: The primary emphasis of this paper is on the mechanics of a computer algorithm for cumulative fatigue damage, Exp. Mech. 17 (1977) 50–56, http://dx.doi.org/10.1007/BF02326426.

[49] L. Coffin, Low cycle fatigue laws, J. Mater. 6 (1971) 388+.

[50] M. Mrsnik, J. Slavic, M. Boltezar, Frequency-domain methods for a vibration-fatigue-life estimation - Application to real data, Int. J. Fatigue 47 (2013) 8–17, http://dx.doi.org/10.1016/j.ijfatigue.2012.07.005.

[51] M.A. Miner, Cumulative Damage in Fatigue, 1945, http://dx.doi.org/10.1115/1.4009458.

[52] J.H. Park, J.H. Song, Detailed evaluation of methods for estimation of fatigue properties, Int. J. Fatigue 17 (1995) 365–373, http://dx.doi.org/10.1016/0142-1123(95)99737.

[53] Z.G. Wang, C. Shi, S.S. Ding, X.F. Liang, Crashworthiness of innovative hexagonal honeycomb-like structures subjected to out-of-plane compression, J. Cent. South Univ. 27 (2) (2020) 621–628, http://dx.doi.org/10.1007/s11771-020-4321-2.